Hindawi
Journal of Nanomaterials
Volume 2017, Article ID 8548041, 11 pages
https://doi.org/10.1155/2017/8548041

Research Article

Dynamic Interferometry Lithography on a TiO_2 Photoresist Sol-Gel for Diffracting Deflector Module

V. Gâté,[1,2,3] L. Berthod,[1,2,3] M. Langlet,[2,3] F. Vocanson,[1] I. Verrier,[1] C. Veillas,[1] A. Kaminski,[4] O. Parriaux,[1] and Y. Jourlin[1]

[1] *Université Lyon, UJM-Saint-Etienne, CNRS, Lab. Hubert Curien UMR 5516, 42023 Saint-Etienne, France*
[2] *Universit Grenoble Alpes, LMGP, 38000 Grenoble, France*
[3] *CNRS, LMGP, 38000 Grenoble, France*
[4] *IMEP-LAHC/PHELMA, Grenoble INP, Grenoble, France*

Correspondence should be addressed to Y. Jourlin; yves.jourlin@univ-st-etienne.fr

Received 18 October 2016; Revised 20 January 2017; Accepted 29 January 2017; Published 9 March 2017

Academic Editor: Xuezhang Xiao

Solar electricity is one of the most promising renewable energy resources. However, the ratio module's cost/energy produced remains a major issue for classical photovoltaic energy. Many technologies have been developed to solve this problem, by using micro- or nanostructuring on the solar cell or on the module. These kinds of structuring are often used as antireflection and light-trapping tools. In the meantime, other solar technologies are considered, such as concentration photovoltaic modules. This article presents a module combining both approaches, that is, nanostructures and concentration, in order to increase the module's profitability. Sol-gel derived TiO_2 diffraction gratings, made by dynamic interferometric lithography, are added on the top of the glass cover to deflect unused light onto the solar cell, increasing the module efficiency.

1. Introduction

Micro- or nanostructuring for light-trapping and antireflect coatings has been studied during the last decade in order to increase solar cell and photovoltaic (PV) module efficiency. A large part of these works is dedicated to decrease reflection at the multiple interfaces of the PV module: most of these structures involve submicrometric patterns, such as diffraction gratings [1–5]. Other structures have been placed under the solar cell in order to reflect the light passing through the cell [6, 7]. To increase the efficiency of solar cell, concentration technologies have been studied and applied. They are able to concentrate the light with a concentration factor up to thousands suns onto a very efficient solar cell. Most of these technologies use expensive optical systems such as Fresnel lenses (Concentrix-Soitec, Amonix) or hyperbolic mirrors (Solfocus, HeliosPV) as well as expensive heterojunction solar cells. Recently, new types of concentrator have been studied, which are able to concentrate the light moderately with a concentration factor from 2 to 300 suns [8–13]. These structures are mostly based on holographic concentrators and diffraction gratings which trap and deflect the incoming light onto the solar cells. This technology led Prism Solar to industrially produce modules based on holographic diffraction gratings trapped between the cover and the back glass, combined with double faces crystalline solar cells. These modules are said to be up to 50% more efficient than regular monofacial crystalline solar cell modules. The technology presented in this paper focuses on diffraction gratings placed on the top of the glass cover to deflect the light to the cell directly or by Total Intern Reflection (TIR). The gratings are made by dynamic interferometric lithography (DIL) onto a TiO_2 xerogel thin film, with a technology developed in our laboratories [14–18]. This technology allows fabricating long and large diffraction gratings directly on a robust material with very interesting optical properties for diffraction gratings. The aim of the module that we have developed is to decrease the area of PV material for a given efficiency or increase the efficiency for a given area of PV material. This work will focus on the conception of a PV

module demonstrator by (i) designing the best diffraction gratings and their best refractive index/thickness couples, (ii) fabricating large TiO_2-based gratings on the top of the glass cover, and (iii) finally testing them under a solar simulator.

2. Grating Fabrication and Experiments

To produce the diffraction gratings, we have used a sol-gel procedure combined with DIL. These two processes enable us to make large TiO_2-based diffraction gratings. The whole sol-gel process has been detailed in previous papers [14, 18], as well as the DIL process [16, 17]. Both processes will be briefly described hereafter.

2.1. Sol-Gel Process. The sol was prepared from titanium alkoxide, titanium ispropoxide orthotitanate (TIPT, from Flucka), complexed by benzoyl acetone (BzAc, from Sigma Aldrich). The final sol was formed from two different sols. The first one (S1) was fabricated by mixing TIPT with BzAc in methanol (MeOH), with a TIPT/BzAc/MeOH molar composition of 1/0.75/20.4. The second sol (S2) was prepared by mixing TIPT, deionized water, HCl, and butyl alcohol (BuOH) as a solvent. The TIPT/H_2O/HCl/BuOH molar ratio of this sol was 1/0.82/0.13/23.9. Before mixing with S1, S2 was aged for two days at room temperature. The final sol obtained after mixing had a BzAc concentration of 0.5 M and a BzAc/TIPT molar ratio of 0.6.

In the present study, films were deposited on 9 cm × 9 cm glass plates (from Saint Gobain) by spin-coating at 1200 rpm. After sol deposition, the samples were naturally dried at room temperature for a few minutes before being baked during 90 minutes at 110°C, which led to the formation a TiO_2 xerogel thin film. In this state, the film was highly soluble in alcohols thanks to TIPT/BzAc complexation. BzAc provides an interesting ability to the film: it makes it sensitive to UVA light, from 340 nm to 380 nm. Insolation of the film by UVA leads to photolysis of the complex, producing species insoluble in alcohols. It yields a solubility contrast between exposed and nonexposed areas, allowing patterning of the film. To strengthen this contrast of solubility, the exposed film was heat treated for 8 minutes at 110°C.

Thin films obtained by this way show good optical properties even after being heat treated for 2 hours at 500°C, as depicted in Figure 1. Figure 1(a) presents the UV-visible transmission spectrum of the bare glass. Figure 1(b) depicts the spectrum of the xerogel film, where one can notice the absorption of BzAc complex around 360 nm. Figure 1(c) shows the spectrum of an UVA exposed xerogel film, where one can notice that the transmission level around 360 nm is slightly higher than in Figure 1(b), since the complex BzAc/TIPT has been partially photolysed. Figure 1((d) and (e)) show the transmission spectra of a TiO_2 film heat treated at 500°C for a one-layer film and a 3-layer film, respectively. One can see that both spectra match that of the glass substrate but they appear to be red shifted due to the TiO_2 UVA absorption that increases when increasing the film thickness. Optical losses that can be observed in the visible range are due to interferences caused by the highly reflective TiO_2-on-glass layer.

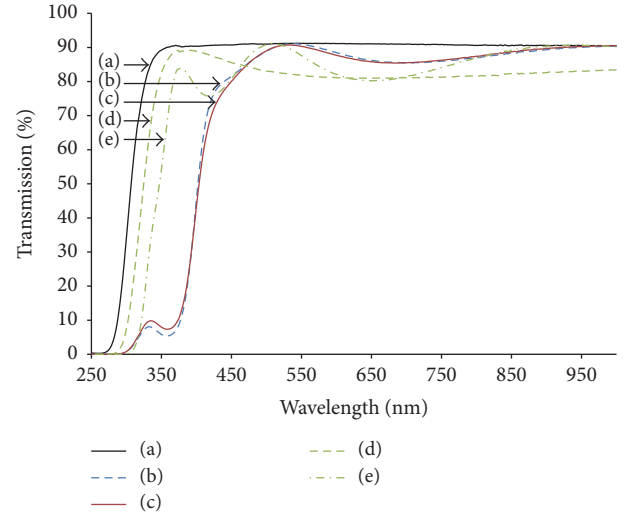

Figure 1: UV-visible spectra: bare glass (a); xerogel coated glass heat treated at 110°C (b); exposed xerogel film on glass (c); single layer xerogel film on glass after heat treatment at 500°C (d); three-layer xerogel film on glass heat treated at 500°C (e).

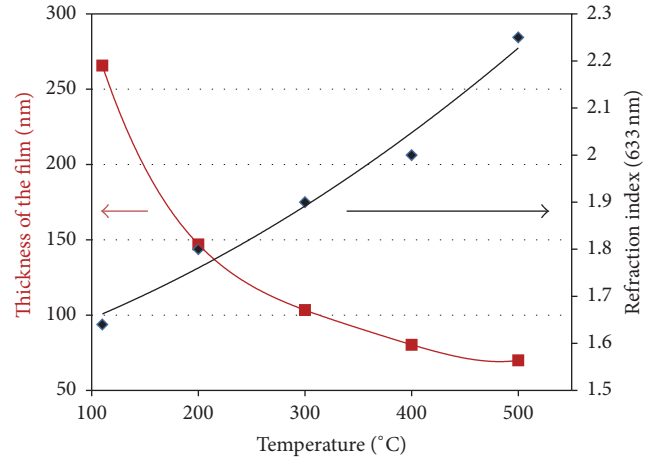

Figure 2: Film thickness and refractive index as a function of the heat treatment from 110°C to 500°C.

The sol-gel film exhibits densification effects while being heat treated. An initially 270 nm thick xerogel film undergoes a thickness reduction down to 70 nm after thermal treatment at 500°C, while, thanks to the densification effects, its refractive index at 633 nm increases from 1.65 to 2.25. Densification of the film, that is, the increase of its refractive index combined with the reduction of its thickness, allows choosing a refractive index/grating depth couple and offers more flexibilities to the xerogel than the TiO_2 PVD process. The behavior of the film during heat treatment is presented in Figure 2.

With this process, it is possible to achieve submicrometric patterns in a titanium dioxide substrate such those we need to build the diffracting deflector.

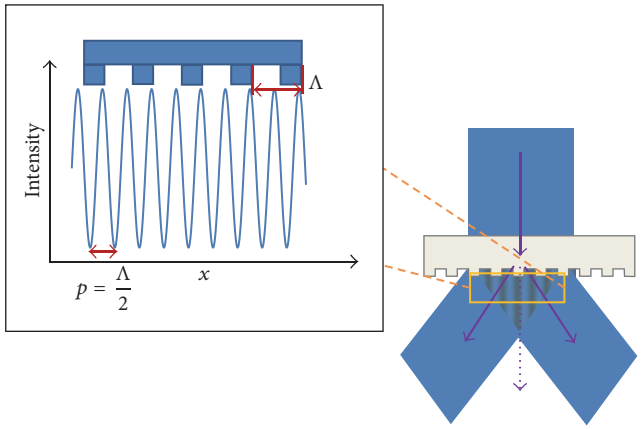

Figure 3: Interference pattern underneath the phase mask in normal condition. The pattern's period is half of the masks.

2.2. DIL Process. The DIL process was based on the use of a phase mask, which was a diffraction grating of period Λ, etched in a transparent substrate (fused silica in this case). The grating was illuminated with a laser beam which was hence diffracted, producing diffraction orders overlapping underneath the mask. In the overlap zone, diffraction orders should interfere together, producing an interferogram which will be used to expose the photosensitive sol-gel layer. When illuminating the grating in normal incidence, the interferogram period should be half of the mask's one (Λ/2), as depicted in Figure 3. The best phase masks are achieved when only two orders are transmitted through the diffraction grating, resulting in a two beams interference pattern. However, such results are very hard to achieve in normal incidence since the 0th order is still remaining, as well as other higher orders such as the 3rd ones. The many orders of interference should thus result in a pattern showing periodicity Λ as well as periodicity Λ/2.

As it will be shown in Section 3, the grating's period needs to be 600 nm; hence a phase mask producing a 600 nm period interferogram has been designed. Unfortunately, since it was not possible to cancel 0th order, the interferogram pattern does not have only a 600 nm period but also a 1200 nm one, which is illustrated by the electric field modulus under the mask in Figure 4(a). The double periodicity caused by the many diffraction orders transmitted through the mask is depicted in Figure 4(b).

The phase mask was illuminated by a line-shaped laser beam to produce a large interference pattern. The substrate was then moved underneath the mask in a direction parallel to the diffraction grating's lines, producing number limited but endless lines of grating into the sol-gel layer.

The DIL system was set in a direct laser writing equipment, Dilase 750 from Kloé [19]. This equipment displays a two-dimensional translation bench, with position accuracy of 100 nm and translation speed ranging from a few microns/second to several tens of millimeters/second. The laser used for exposure was a Genesis series from Coherent with 100 mW power and 355 nm wavelength.

2.3. Characterizations. The diffraction gratings were characterized by Atomic Force Microscopy (AFM, Agilent 5500 LS in tapping mode) and Scanning Electron Microscopy (FEG-SEM, FEI Novanano SEM 200). The films were characterized by ellipsometry (Gaertner L116B ellipsometer) at a 633 nm wavelength and UV/visible spectroscopy in transmission (Perkin Elmer Lambda 900 UV/Vis/IR).

The module demonstrator has been tested with a solar simulator from Sinton Instruments: FCT-400 Flash Cell Tester. The glass cover equipped with the grating on its top was deposited on a polysilicon solar cell with a glycerol layer between them acting as an index matcher. Measurements were done under AM 1.5. Two cases can be distinguished: solar cell only, where the diffraction grating is obliterated by a plate to prevent its actions, and solar cell with diffraction grating where the grating is no longer obliterated and can diffract the light. The diffraction grating was cumulatively heat treated on the glass substrate at 110°C, 200°C, 300°C, 400°C, and 500°C during 2 h at each temperature. Solar simulator tests and AFM measurements were carried out after each heat treatment.

3. Module's Design

This work is focused on the module level: the aim is to deflect the nonused light on the solar cell, using a concentrating effect induced by diffraction gratings put on top of the glass cover and placed next to the solar cell, as depicted in Figure 5. This extra flow of light should increase the solar cell photo current and should produce extra electricity while maintaining the same area of photovoltaic material. The concentration effect is brought by the diffraction grating which should angularly split the incoming light wavelengths and bring wanted wavelength range to the solar cell either directly or by TIR. To optimize the concentration, we need to optimize the grating's characteristic while keeping fixed module parameters. Figure 5 represents the module's principle with the main parameters: the 9 cm large solar cell is placed underneath the glass cover which is 3.2 mm thick. The edge of the glass is covered by a 20 mm large diffraction grating. The incoming light is diffracted with an angle θ for the −1st order. These parameters will remain constant along the following study.

The first part to achieve is to design the most efficient diffraction grating. To do so, a range of wavelengths has been set, from 600 nm to 800 nm, which may differ from a solar cell technology to another. The grating needs to diffract the whole wavelength range.

The first step is to design the diffraction grating in order to bring the required properties. To do so, the grating's period is calculated through the grating equation:

$$\Lambda = \frac{\lambda}{n \sin(\theta_d)}, \quad (1)$$

where Λ is the grating period, λ is the wavelength coming through the diffraction grating, n is the refractive index of medium, and θ_d is the angle of the diffracted orders. Since the optical wavelength range was set, the two limits,

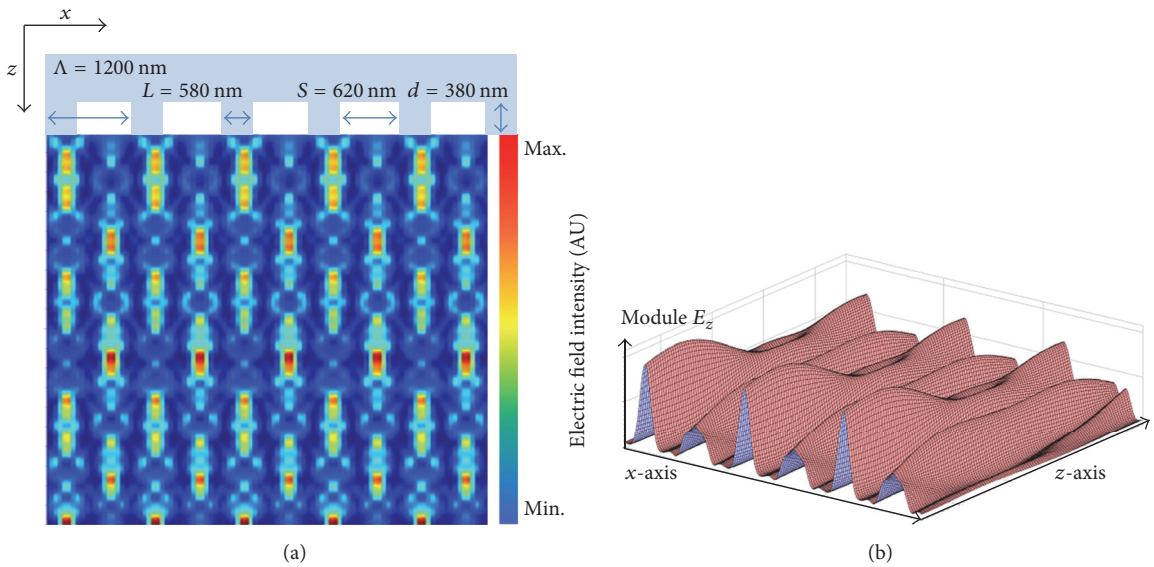

Figure 4: Scheme of the phase mask's electric field intensity as a function of z-axis.

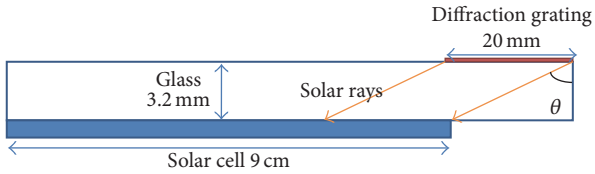

Figure 5: Module's parameters. The 2 cm large diffraction grating (red) is placed on the top of the 3.2 mm thick glass cover and deflects the light on a 9 cm large solar cell (blue).

that is, 600 nm and 800 nm, should be considered. The grating is to be set on glass, so that the refractive index n is considered equal to 1.5. For a 800 nm wavelength, θ_d must be inferior to 90° so that the rays can be diffracted. Using (1), the grating's period has thus to be superior to 533 nm. Considering a 600 nm wavelength in (1), for the light coming on the far edge of the grating to be deflected directly on the solar cell, a period inferior to 414 nm is required, which is obviously incompatible with the previous requirement. To solve this issue, we used TIR to bring the "blue part" of the wavelength range to the solar cell, the glass cover being used as a waveguide for the rays. The TIR requirement brings an angular condition to the diffracted angle. Using the Snell-Descartes law, we can calculate θ_d compatible with TIR in the glass. The calculation gives $\theta_d > 41.8°$. Injecting this condition in (1), with $\lambda = 600$ nm, a new requirement on the grating's period is set: Λ has to be inferior to 600 nm. Hence, the range of period available for the light to be deflected was 533 nm $< \Lambda <$ 600 nm. The principle of the module is shown on Figure 6: the module is represented on cross section and illustrates a solar cell framed by two diffraction gratings on both sides. The 800 nm wavelength (green arrows) is directly deflected to the cell, while the 600 nm wavelength (blue arrows) has to be guided by TIR.

These predictions of TIR to bring the "blue part" on the solar cell are not completely true. Indeed, these wavelengths guided in the glass will diffract due to the presence of the diffraction grating on the surface (coupling/uncoupling). However, these leaks, present at the grating interface, were measured and modeled (not presented here) and are very low.

To discriminate the best period, simulations have been computed with a Rigorous Coupled Wave Analysis software, named MC gratings [20]. The calculations were done for the efficiency of ±1st diffraction orders for period Λ ranging from 533 nm to 600 nm, incidence angles ranging from −15° to +15°, and for transverse electric (TE) and transverse magnetic (TM) polarization. Figure 7 represents the −1st order's efficiency as a function of the wavelength and the grating period. The TiO_2 xerogel grating considered here has a depth of 300 nm and a refractive index of 1.65. The wavelength ranges from 600 nm to 800 nm and the grating's period goes from 400 nm to 1000 nm. In this diagram, red indicates a higher −1st-order efficiency. Hence simulations confirm that the wavelength range is not entirely diffracted by gratings whose period is between 533 nm and 600 nm.

As explained, simulation has been obtained for several incidence angles ranging between −15° and +15° and for transverse electric (TE) and transverse magnetic (TM) polarization. The results were integrated over the wavelength range to obtain a curve representing the grating's efficiency as a function of the grating's period. Such curve is presented on Figure 8. Figure 8(a) depicts the integrated value of the −1st order's efficiency, in arbitrary units, over the wavelength's range as a function of the diffraction grating's period in TE polarization. Figure 8 ((b) and (c)) depicts the TM polarization and the mean of (TE + TM)/2 polarization, respectively. TE curve continuously increases to a maximum around 670 nm, TM curve has a maximum around 570 nm, and the mean curve has the same maximum as TE. As we have seen previously, the available range of period for the diffraction

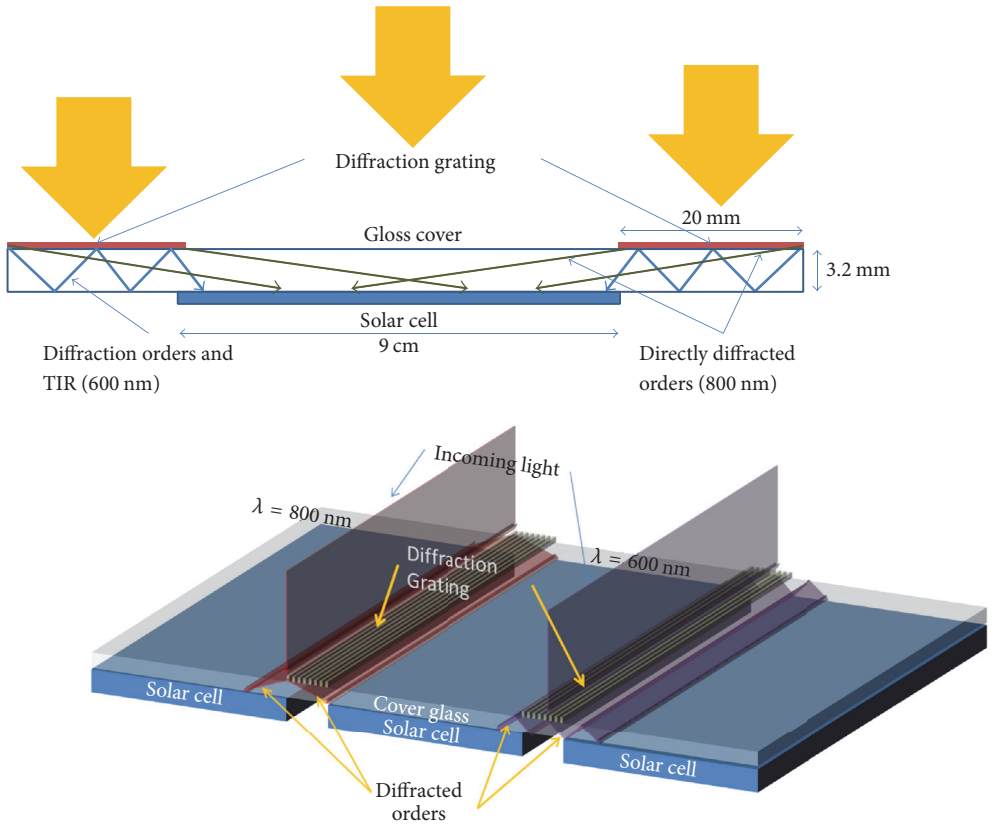

FIGURE 6: Grating deflector module. The gratings are placed between the cells on the top of the glass cover. The 800 nm wavelengths (red) are directly redirected on the cell, while 600 nm wavelengths (purple) are redirected by TIR.

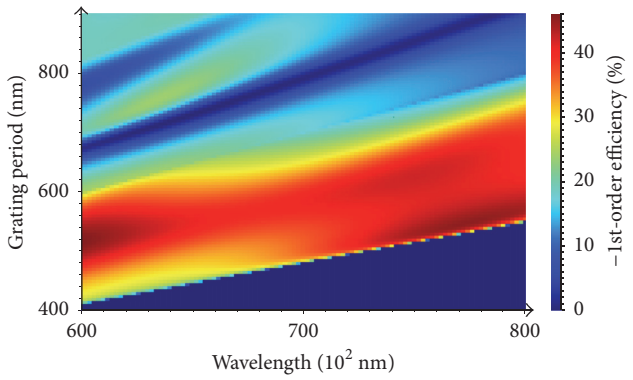

FIGURE 7: Power in the −1st order for diffraction grating in normal incidence and TE polarization, as a function of the grating's period and the wavelength. The redder the color is, the more powerful the −1st order is.

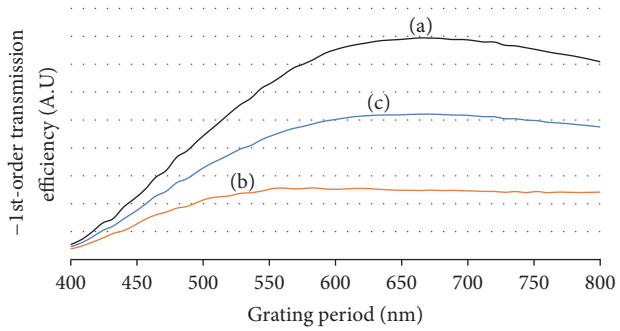

FIGURE 8: Efficiency (in arbitrary units) of the −1st order for 600 nm period diffraction grating in normal incidence as a function of the wavelength. Curve (a) is for TE polarization, curve (b) is for TM polarization, and curve (c) is for TE + TM.

grating is from 533 nm to 600 nm. Hence, the grating's period has to be set in order to reach the maximum of intensity possible in this range, which means that it will be set to 600 nm.

Figure 9 shows efficiency of ±1st diffraction orders in TE polarization and that of the sum of the two orders as a function of the angle of incidence in the case of a grating period of 600 nm. Efficiency variations of +1st and −1st orders are symmetrical to each other with respect to the 0° angle of incidence. For angles of incidence in the −15°/15° range, their efficiency lies between 24% and 44%, the maximal value being obtained with an angle of −7° (7°) for −1st (+1st) order. In normal incidence, ±1st orders efficiency is 37%. The sum of both orders shows a maximum efficiency of 74% for an incidence of 0°. This efficiency weakly varies in the −10°/10° range and then it decreases continuously when the incidence goes away from the normal to reach a value of 51%

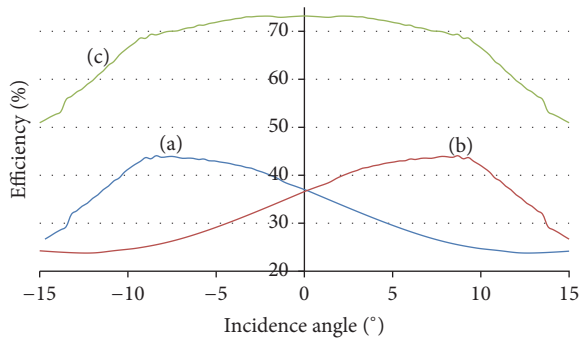

FIGURE 9: Efficiency of (a) the −1st order, (b) the +1st order, and (c) the sum of the two orders as a function of the incidence angle for a 600 nm period, 300 nm thickness, and 1.65 refractive index TiO_2 grating.

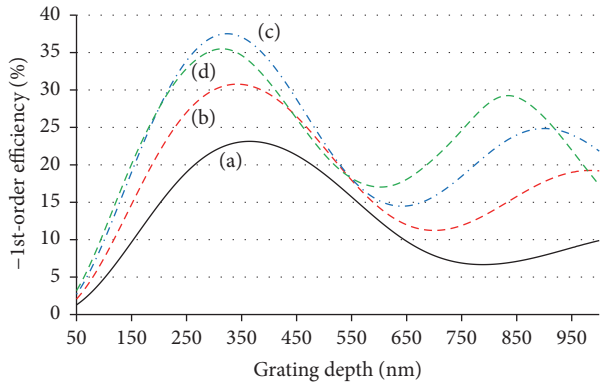

FIGURE 10: Efficiency of the −1st order of 600 nm period diffraction grating in normal incidence as a function of the grating's depth for several refractive indexes n: (a) $n = 1.6$; (b) $n = 1.8$; (c) $n = 2$; (d) $n = 2.2$.

at ±15°. These data demonstrate a relatively high efficiency and relatively good angular tolerance of the grating over the entire range of angles studied.

Considering our TiO_2 sol-gel material and the possible grating depth reachable, we can investigate the best agreement between the grating's depth and the refractive index. Figure 10 depicts the −1st order's efficiency of a 700 nm beam diffracted by a 600 nm period sinusoidal diffraction grating, in normal incidence, for several refractive indexes ranging from 1.6 to 2.2. We can see that the maximum arises in any case for a depth lying between 250 nm and 350 nm. The best efficiency is reached for $n = 2$ and a 300 nm depth.

After calculations, considering the reachable thickness/refractive index couples, ±1st orders are thus expected to bring a gain of current of 70%. However, if the parameters described above seem to be the best ones for the device's purpose, the experimentally reachable parameters are not necessarily the same as it will be shown in the next section.

4. Experimental Results

4.1. Diffraction Gratings. Diffraction gratings were fabricated on 9 cm × 9 cm glass substrate from Saint Gobain, which is used to cover solar cells in PV modules. Diffraction gratings of 9 cm × 2 cm size were produced through sol-gel and DIL process. Xerogel TiO_2 thin films were insolated by a 2 cm long interferogram, presented in the previous paragraph, while moving underneath at a speed of 0.01 mm/s. The gratings presented heterogeneities at the millimeter scale caused by interferences due to multireflections between the incoming laser beam, the mask, and the highly reflective TiO_2–on-glass substrate. Grating lines also presented some reliefs in their length as depicted in Figure 11.

Because of the presence of undesired diffraction orders, such as 0th and ±3rd orders, the interferogram period was double with $\Lambda_1 = 1200$ nm and $\Lambda_2 = 600$ nm as detailed previously. This double period is then reproduced in the sol-gel resist owing to its highly linear behavior, as illustrated in Figure 11(a). Hence, the 1200 nm period brings unwanted ±1st diffraction orders which would not be present for a single period of 600 nm. This will reduce the efficiency of the grating to deflect the light on the solar cell. However, despite this double periodicity in the TiO_2 xerogel grating, diffraction effects are clearly visible in Figure 11(b). This grating is printed on a glass substrate and has a 2 cm width and a 9 cm length as the length of the solar cell.

The AFM profile's evolution of gratings heat treated cumulatively at 110°C, 200°C, 300°C, 400°C, and 500°C for two hours is illustrated in Figure 12. For the reasons discussed previously, after a heat treatment at 110°C, the diffraction grating has a superposition of a primary period of 1200 nm and a secondary period of 600 nm leading to a depth of 140 nm in the primary lines, which depicts the targeted periodicity of 600 nm (Figure 12(a)). It may be noted that this modulation is weaker and less regular than in the simulation presented in Figure 4, which implies that, in the tests presented here, the resin was probably slightly overirradiated. As mentioned previously, the cumulative heat treatments lead to densification effects resulting in a reduction in the gratings thickness.

These effects of densification also lead to changes in the superstructure. After a treatment at 200°C, the modulation is reflected by a reduction in the depth of the primary lines (Figure 12(b)). From 200°C to 300°C, the depth decreases again (Figures 12(b) and 12(c)). In the same time, there is a significant reduction in the width and thickness of the main 1200 nm periodicity relief, which probably depicts the effects of lateral and vertical densification. These effects are again amplified after heat treatment at 400°C and 500°C (Figures 12(d) and 12(e)).

4.2. Module Efficiency. Efficiency of the module endowed with TiO_2 gratings was assessed by tests performed in a solar flux simulator after each cumulative heat treatment. The demonstrator module was assembled by placing the structured glass on a polycrystalline silicon solar cell, with a glycerol layer at the interface that provided an index matching between the glass and the cell. The module is shown on Figure 13.

The module efficiency was measured under AM 1.5 and two architectures were considered: the first one (A) was a reference to measure the parameters obtained for the cell

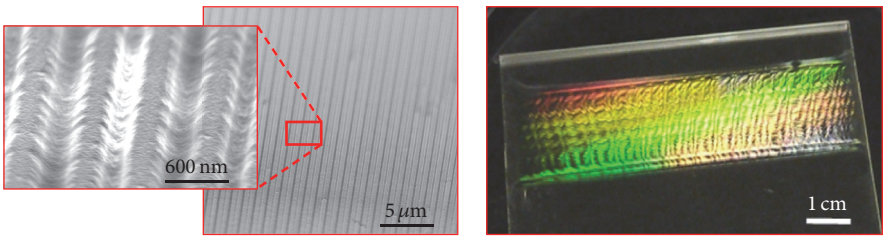

Figure 11: SEM images of 600 nm/1200 nm periods xerogel diffraction gratings made by DIL (a) and optical micrograph of a 2 cm × 9 cm diffraction grating made by DIL (b).

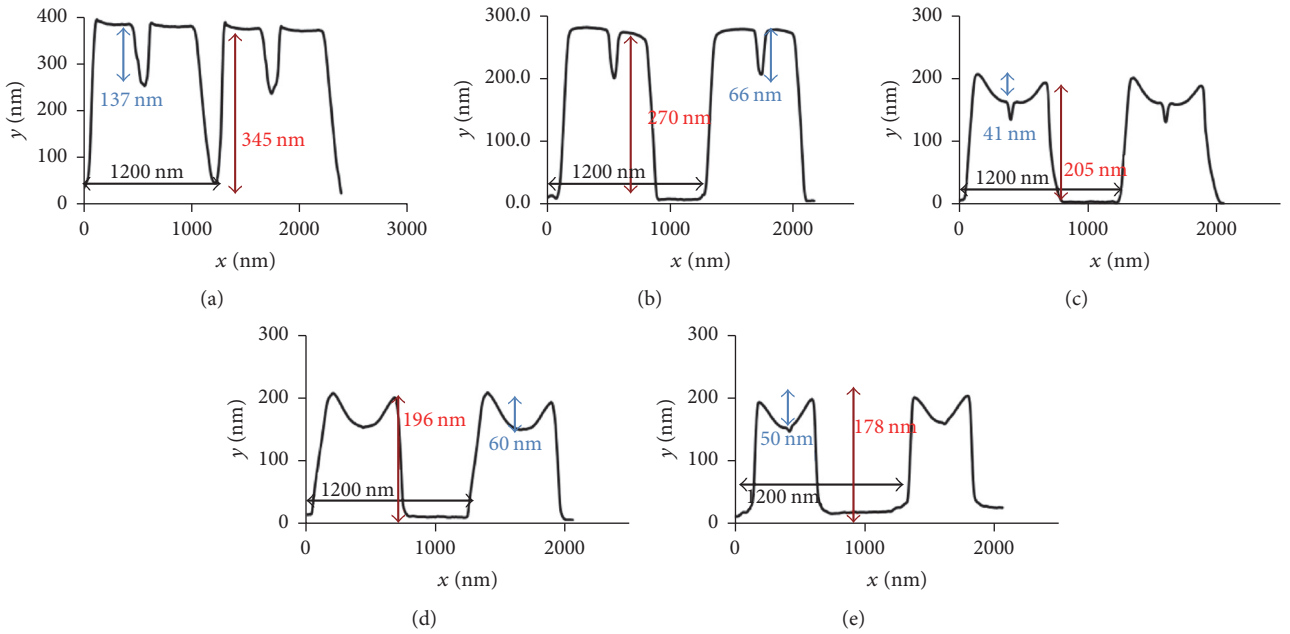

Figure 12: AFM profiles of double period diffraction grating made by DIL after several cumulative annealing treatments: (a) 2 h at 110°C; (b) (a) + 2 h at 200°C; (c) (b) + 2 h at 300°C; (d) (c) + 2 h at 400°C; (e) (d) + 2 h at 500°C.

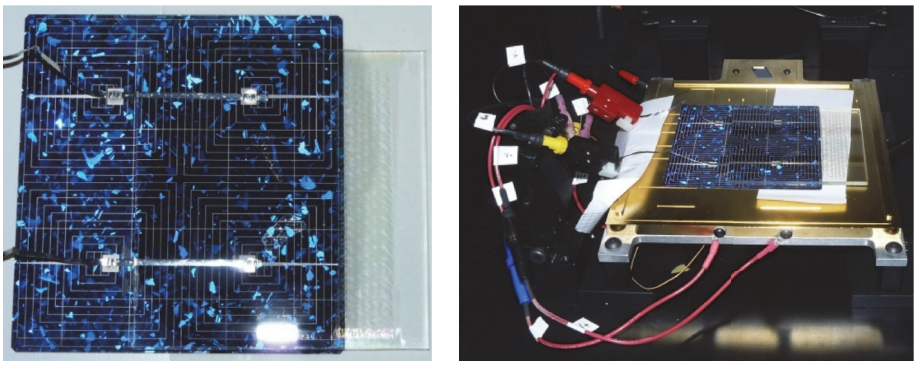

Figure 13: Module demonstrator. Solar cell with its diffraction grating structured cover glass (a) and the same cell inside the solar simulator (b).

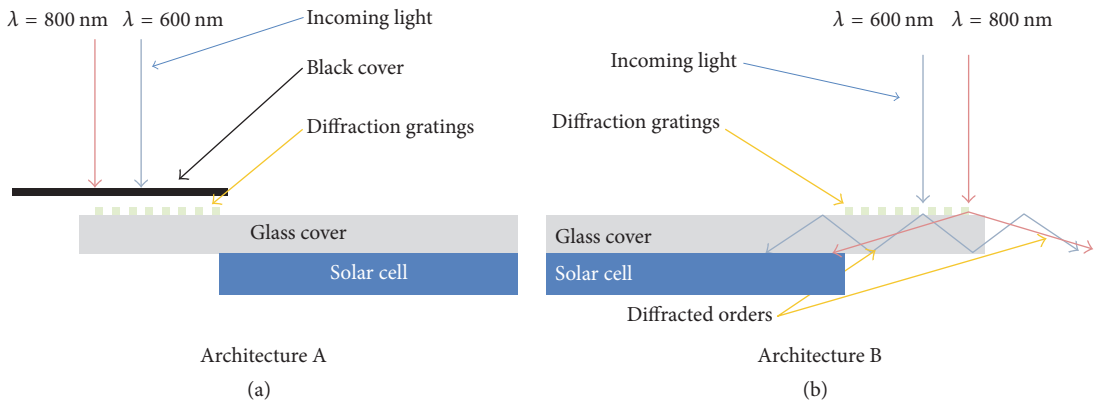

FIGURE 14: The two types of setup for the solar tests: architecture A (a) shows a side view of the module with a black cover on the diffraction grating in order to prevent the light from illuminating it; architecture B (b) is the same without the black cover to allow the grating to deflect the light.

alone and the second one (B) was a measurement of the parameters with the diffraction grating being enlightened. Both architectures are illustrated in Figure 14. These measurements were done after each heat treatment so that the parameters could be analyzed in relation to the gratings morphology derived by AFM.

The short-circuit current (I_{sc}), the open circuit tension (V_{oc}), and the fill factor (FF) were measured as well as $I(V)$ responses. The open circuit tension remained constant at 0.561 V along all the heat treatments and for both architectures. However, I_{sc} was always increased from architecture A to architecture B.

In the case where the grating is not active (architecture A), a short-circuit current of 2.85 ±0.02 A was measured after each heat treatment. The ±0.02 A uncertainty is related to sample conditioning (positioning, contacts, etc.) during the measurements. However, this error does not affect the comparison between measurements with or without grating since; after each heat treatment, conditioning is not modified from architecture A to architecture B. Figure 15 illustrates the variations of ΔJ_{sc}, that is, the evolution of the short-circuit current density ($\Delta I_{sc} = I_{scA} - I_{scB}$ per surface unit) when the grating becomes active, as a function of the heat treatment temperature. For each temperature, we note that the presence of the grating increases the short-circuit current. This increase is relatively weak for temperatures between 110°C and 300°C, with $\Delta J_{sc} = 1.05 \pm 0.15$ mA/cm^2, and it increases significantly at temperatures of 400°C and 500°C, with $\Delta J_{sc} = 1.79 \pm 0.1$ mA/cm^2. These observations demonstrate that, even with nonoptimized etching conditions, as illustrated in Figure 12, it is possible to increase the short-circuit current thanks to the presence of the grating. Figure 15 shows that this effect results in a significant increase in the conversion efficiency of the solar module, which ranges from 0.4 ± 0.1% after treatment at 110–300°C up to 1.05±0.05% after treatment at 400–500°C.

In the concept proposed here, the grating is set on a solar cell free zone, and therefore it aims to reduce the number of cells. It is interesting to compare the power produced by a

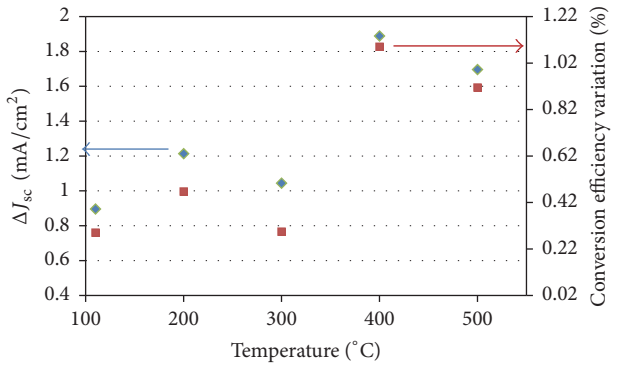

FIGURE 15: Influence of heat treatment on the short-circuit current density (blue) and conversion efficiency (red) when passing from architecture A (inactive grating) to architecture B (active grating).

solar cell that has received the light deflected by a grating of surface S to the power that would be produced by a solar cell, with the same surface S, directly exposed to solar radiation. Considering an incident power P_i AM 1.5 of 1000 W/m^2, a solar cell of surface S and efficiency η (10.2% for cells considered here) can provide an electrical power P_f (in W):

$$P_f = S \times P_i \times \eta. \quad (2)$$

By comparing the measured power when testing architecture A (P_A) and B (P_B) and the power deflected by a grating of surface S (P_{RD}), we obtain

$$P_{RD} = P_B - P_A. \quad (3)$$

One can thus calculate R_{Cell} ratio (in %) to compare the power obtained using a grating of surface S with the power directly produced by a cell of the same size:

$$R_{cell} = \frac{P_{RD}}{P_f} \times 100. \quad (4)$$

Figure 16 shows the variations of R_{Cell} ratio as a function of the heat treatment temperature. This figure depicts two

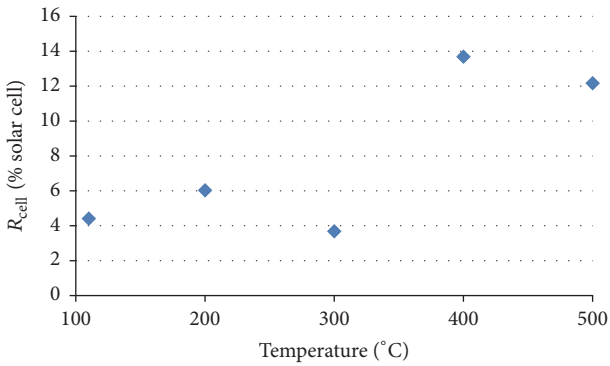

FIGURE 16: Effect of heat treatment on R_{Cell} ratio describing the power gain obtained by a grating of surface S compared to the power produced by a cell of same surface directly illuminated by the solar radiation.

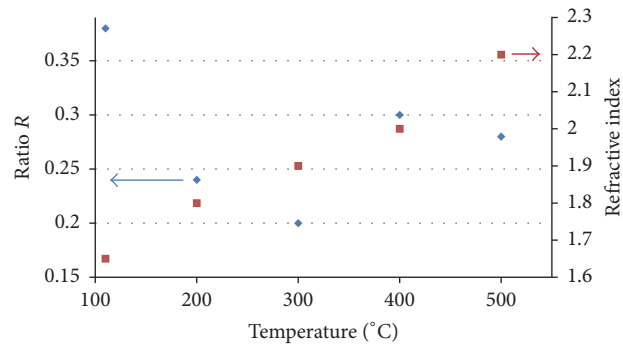

FIGURE 17: Evolution with heat treatment temperature of the ratio $R = p/h$ between the depth and height of the superstructure designs (blue) and the refractive index of the grating (red).

types of behaviors that correlate very well those shown in Figure 15. For a temperature between 110 and 300°C, the power gain provided by the ±1st orders diffracted by the grating is around 4 to 6% compared to the power that would be produced by a cell directly illuminated. For a treatment at 400 or 500°C, this power gain is multiplied by a factor of around 2.5, corresponding to a value in the range of 12–14%. This observation means that, for these latter heat treatments, the amount of deflected photons is much larger, but this gain is still low compared with the one produced by a cell directly illuminated.

5. Discussion

It is necessary to discuss the effects of the postetching heat treatments which do not necessarily go in the direction predicted by the simulations. Indeed, these latter predict an optimal diffractive power, that is, an optimum electrical power gain, for gratings with a refractive index of about 2 and a thickness of about 300 nm. But our best experimental results are obtained for heat treatments at 400 or 500°C, which yield an index greater than or equal to 2 (Figure 2) and a grating thickness of 200 nm or less (Figure 12). These phenomena can be discussed in conjunction with the optical properties of the studied gratings.

As noted above, heat treatment significantly alters the dimensions and profile of photoetched gratings and the annealing effects provide gratings closer to those modeled. Particularly, they lead to the amplification of a submicrometric modulation grafted onto the initial micronic patterns. It seems that the amplification of these modulations with heat treatment temperature plays a role in the diffraction, leading to a more efficient deflection of light toward the solar cell power. The patterns obtained after different heat treatments can be characterized by the ratio R between the modulation depth (p) and the height (h) of the main relief ($R = p/h$). The values of R deduced from AFM data of Figure 12 for each heat treatment are illustrated in Figure 17. The R ratio decreases significantly when the temperature increases from 110°C to 300°C, and then it increases again up to relatively similar values after treatment at 400°C and 500°C. In addition, we also saw in Figure 2 that the effects of thermoinduced densification result in a continuous increase of the film refractive index, from a value of 1.65 (110°C) up to a value of 2.2 (500°C). We can consider that, for an equivalent annealing temperature, the refractive index of a photopatterned grating is close to that of a nonetched film.

It is possible that the amplification of submicron modulations, characterized by an enhanced R ratio, plays an important role in the diffracting grating power. This parameter should act in conjunction with the refractive index for which a higher value is expected to increase the diffraction efficiency. These aspects may explain the data illustrated in Figure 16. This figure shows that, for annealing temperatures between 110°C and 300°C, the effect of gratings on the power delivered by the module is relatively and comparably weak. In this temperature range, it is likely that the increase in refractive index with temperature is offset by the significant drop in the R ratio. In contrast, Figure 16 shows that the effect of gratings on the power supplied by the cell is more important, and again very similar, for annealing temperatures of 400°C and 500°C. In this temperature range, it seems that the diffracting efficiency is jointly promoted by the increased of both the R ratio and the refractive index. At this stage, it is not possible to provide a more detailed analysis of experimental data, and it would be necessary to perform additional tests to deepen understanding of the effects induced by submicron superstructures on the power produced by the cell. However, we can complete this discussion by focusing on the effect induced by the micrometric periodicity of the main patterns of our gratings.

This complementary discussion is supported by simulations performed with "MC gratings" in TE polarization, as illustrated in Figure 18 for an index of 2. Figure 18(a) shows the −1st-order efficiency of an ideal grating with a period of 600 nm. Efficiency is similarly high on the whole range of investigated wavelengths (600–800 nm). However, our samples are in fact characterized by a main periodicity of 1200 nm that provides additional unwanted diffracted orders, the 0th one being the most intense, which result in a loss of the incident energy deflected toward the solar cell. For example, for a wavelength of 600 nm, the calculations show

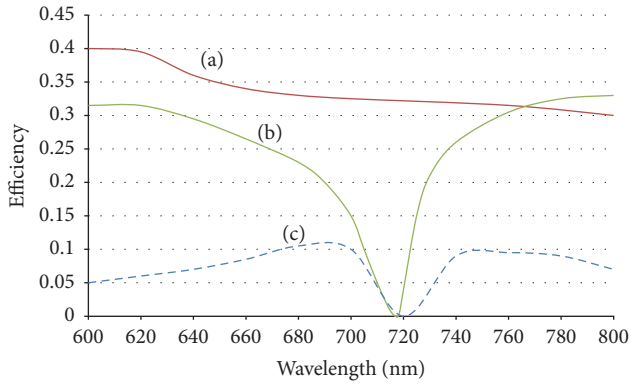

Figure 18: Simulation of the grating efficiency (a) for the −1st order and a grating period of 600 nm, (b) for the −2nd order and a grating period of 600 nm, and (c) for the −1st order and a double grating period 1200 nm/600 nm close to the one obtained after heat treatment at 400°C.

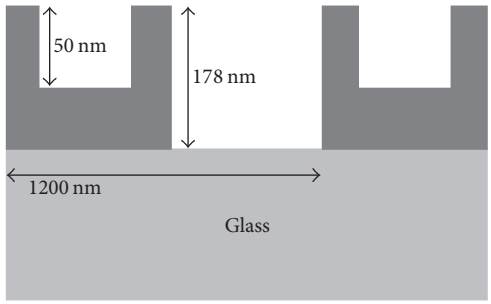

Figure 19: Grating used to simulate the real case with MC gratings profile.

that the periodicity produces very intense ±1st orders, but these orders are diffracted with an angle of 21° to the normal, that is, a value weaker than that required to guide light by TIR. These orders are thus mainly transmitted through the glass without illuminating the cell.

To precisely know how the periodicity of 1200 nm decreases the diffraction efficiency and thus the photovoltaic module efficiency, a simulation with MC gratings was also performed in the case of a dual period 600/1200 nm whose profile is presented in Figure 19. Note that this concept of dual period actually corresponds to an idealized case since here we cannot strictly consider a periodicity of 600 nm. For this dual periodicity, the curves (b) and (c) of Figure 18 illustrate the efficiency of the −1st and −2nd orders, respectively. Indeed, for a period of 1200 nm, the ±2nd orders are diffracted with the same angle as the ±1st order produced in the case of a 600 nm period grating. Figure 18 ((b) and (c)) leads to several conclusions. For wavelengths near 600 and 800 nm, the diffraction efficiency of the −1st order is still important in the case of the dual period but, with the 1200 nm period being mainly predominant in our samples, we have seen that the diffraction angle is not consistent with light guiding by TIR. Besides, the diffraction efficiency of the −2nd order arising from the periodicity of 1200 nm, which may be favorable for our application, is itself extremely small. Finally, the diffraction efficiency of both −1st and −2nd orders is also very low or even close to zero for wavelengths around 700 nm.

All these considerations can explain why, in the present circumstances, only a small portion of the light is actually used for photovoltaic conversion. But many potential optimizations still remain open, leaving these considerations also augur the potential to significantly increase the solar gain in future studies.

6. Conclusion

It is obviously not yet possible to conclude on the economic validity of the concept presented here but only on its feasibility. On the basis of these first demonstrators and preliminary feasibility tests, many optimizations can be envisaged, which especially rely (i) on optimization of the diffracting gratings, which have not been burned by the best conditions (overexposure, predominant micrometer periodicity, etc.), and (ii) on the fact that gratings have been arranged on only one side of the cell but, in a real device, the energy input would be greatly amplified by arranging gratings on all four sides.

Further studies should be performed in these directions. At this stage, it will be possible to assess whether cost criteria (additional cost related to the structure compared to the intrinsic cell cost) justify reducing solar cell surfaces and replacing them with diffraction gratings, even though these gratings would not provide the same power increase as obtained by illuminating a cell directly.

Conflicts of Interest

The authors declare that there are no conflicts of interest regarding the publication of this paper.

Acknowledgments

The authors would like to thank Stephanie Reynaud, David Riassetto, Koceila Yadel, and the French Rhone-Alpes Region. The authors thank Philippe Voarino, from INES (Institut National de l'Energie Solaire) CEA/LITEN, for his experimental support and measurements as well as his modules specifications.

References

[1] C. Bauer and H. Giessen, "Light harvesting enhancement in solar cells with quasicrystalline plasmonic structures," *Optics Express*, vol. 21, no. 3, pp. A363–A371, 2013.

[2] J. Chen and K. Sun, "Nanostructured thin films for antireflection applications," *Thin Solid Films*, vol. 519, no. 15, pp. 5194–5198, 2011.

[3] Y. Kanamori, E. Roy, and Y. Chen, "Antireflection sub-wavelength gratings fabricated by spin-coating replication," *Microelectronic Engineering*, vol. 78-79, no. 1–4, pp. 287–293, 2005.

[4] S.-S. Lo, C.-C. Chen, F. Garwe, and T. Pertch, "Broad-band antireflection coupler for a : SSSi thin-film solar cell," *Journal of Physics D: Applied Physics*, vol. 40, no. 3, pp. 754–758, 2007.

[5] V. K. Narasimhan and Y. Cui, "Nanostructures for photon management in solar cells," *Nanophotonics*, vol. 2, no. 3, pp. 187–210, 2013.

[6] A. Čampa, J. Krč, F. Smole, and M. Topič, "Potential of diffraction gratings for implementation as a metal back reflector in thin-film silicon solar cells," *Thin Solid Films*, vol. 516, no. 20, pp. 6963–6967, 2008.

[7] L. Zhao, Y. H. Zuo, C. L. Zhou, H. L. Li, H. W. Diao, and W. J. Wang, "A highly efficient light-trapping structure for thin-film silicon solar cells," *Solar Energy*, vol. 84, no. 1, pp. 110–115, 2010.

[8] J. M. Castro, J. Brownlee, Y. Luo et al., "Spatial-spectral volume holographic systems: resolution dependence on effective thickness," *Applied Optics*, vol. 50, no. 7, pp. 1038–1046, 2011.

[9] J. M. Castro, D. Zhang, B. Myer, and R. K. Kostuk, "Energy collection efficiency of holographic planar solar concentrators," *Applied Optics*, vol. 49, no. 5, pp. 858–870, 2010.

[10] T. M. De Jong, D. K. G. De Boer, and C. W. M. Bastiaansen, "Diffractive flat panel solar concentrators of a novel design," *Optics Express*, vol. 24, no. 14, pp. A1138–A1147, 2016.

[11] R. K. Kostuk, J. Castillo, J. M. Russo, and G. Rosenberg, "Spectral-shifting and holographic planar concentrators for use with photovoltaic solar cells," in *High and Low Concentration for Solar Electric Applications II, 66490I*, vol. 6649 of *Proceedings of SPIE*, 8 pages, San Diego, Calif, USA, September 2007.

[12] J. E. Ludman, "Holographic solar concentrator," *Applied Optics*, vol. 21, no. 17, pp. 3057–3058, 1982.

[13] J. E. Ludman, J. Riccobono, I. V. Semenova et al., "The optimization of a holographic system for solar power generation," *Solar Energy*, vol. 60, no. 1, pp. 1–9, 1997.

[14] S. Briche, Z. Tebby, D. Riassetto et al., "New insights in photopatterned sol-gel-derived TiO_2 films," *Journal of Materials Science*, vol. 46, p. 1474, 2011.

[15] V. Gâté, G. Bernaud, C. Veillas et al., "New industrial and innovative writing machine for the fabrication of sol-gel TiO_2 based sub-micrometric period diffraction gratings," in *Proceedings of the Micro-Optics*, Proceedings of SPIE, Brussels, Belgium, April 2012.

[16] V. Gâté, G. Bernaud, C. Veillas et al., "Fast dynamic interferometric lithography for large submicrometric period diffraction gratings production," *Optical Engineering*, vol. 52, Article ID 091712, 2013.

[17] P. Müller, Y. Jourlin, C. Veillas et al., "On-the-fly writing of a long grating phase mask," *Optical Engineering*, vol. 50, Article ID 038001, 2011.

[18] O. Shavdina, L. Berthod, T. Kämpfe et al., "Large area fabrication of periodic TiO_2 nanopillars using microsphere photolithography on photopatternable based sol-gel," *Langmuir*, vol. 3, p. 7877, 2015.

[19] KLOE Company, http://kloe.fr/equipement/en/dilase-750.

[20] N. Lyndin, "Modal and C Methods Grating Software," December 2012, http://www.mcgrating.com/.